Thermodynamic, Kinetic, and Conformational Properties of a Parallel Intermolecular DNA Triplex Containing 5′ and 3′ Junctions†

Juan Luis Asensio,‡ Harvinder S. Dosanjh,§ Terence C. Jenkins,*,|| and Andrew N. Lane*,‡

Division of Molecular Structure, National Institute for Medical Research, The Ridgeway, Mill Hill, London NW7 1AA, U.K., CRC Biomolecular Structure Unit, Institute of Cancer Research, Sutton, Surrey SM2 5NG, U.K., and School of Chemical and Life Sciences, University of Greenwich, Wellington Street, Woolwich, London SE18 6PF, U.K.

Received January 8, 1998; Revised Manuscript Received August 31, 1998

ABSTRACT: The interaction of the 11-mer oligodeoxypyrimidine d(TCTTCTUTCCT) with the 17 bp duplex d(CGCT**AGAAGAAAGGA**CG)·d(CG**TCCUTTCTTCT**AGCG) in forming an intermolecular DNA triplex has been examined in solution by surface plasmon resonance (SPR), UV thermal denaturation, circular dichroism (CD), and NMR methods. Thermodynamic data were also acquired for the shorter 15 bp target duplex d(CGCT**AGAAGAAAGGA**)·d(**TCCUTTCTTCT**AGCG), which forms a 3′ flush-ended parallel triplex. CD titrations at pH 5 gave a triplex → (duplex + strand) dissociation constant K_d of 0.5 μM at 15 °C and ∼2 μM at 25 °C for both the 11−15·15 and 11−17·17 systems, in agreement with analysis of the UV melting data and a direct calorimetric measurement. In contrast, the "apparent" K_d value determined by SPR was 10−20-fold smaller. The rate constant for dissociation (k_d) of the third strand from the triplex was found to be ∼0.0002 s^{-1} at 25 °C by SPR. The rate constant for exchange between the triplex and duplex states determined by NMR was ∼2 s^{-1} at 40 °C. The dissociation kinetics measured by SPR are considerably underestimated, which largely accounts for the poor estimation of K_d using this technique. Extensive ^{1}H NMR assignments were obtained for both the 17 bp DNA duplex and the triplex. Large changes in chemical shifts were observed in the purine strand of the host duplex, but only small shift changes were induced in the complementary pyrimidine strand. Dramatic differences in shifts were observed for the G and A residues, especially in the minor groove, consistent with only small, localized conformational changes in the underlying duplex. The magnitude of the shift changes decreased to baseline within one base of the 3′ triplex−duplex junction and over two to three bases at the 5′ junction. Chemical shift changes at the 5′ junction suggest small conformational anomalies at this site. COSY and NOESY spectra indicate that the nucleotides are in the "S" domain in both the triplex and duplex states. These data rule out major conformation changes at the triplex−duplex boundaries. NOEs between pyrimidines in the third strand and those in the duplex showed proximity for these bases in the major groove, which could be ascribed to buckling of the Hoogsteen bases out of the plane of the Watson−Crick base pairs.

The targeting of duplex DNA by small molecules and by oligonucleotides can be an effective means of externally regulating the expression of specific genes, by the "antigene approach" (*1*). Although small ligand molecules such as intercalators and minor groove binders have been used clinically for many years, these agents generally suffer from either poor sequence specificity or only modest affinity (*1*, *2*). More recently, it was realized that the formation of a DNA triple helix (triplex), where a third DNA strand is bound in the major groove through specific hydrogen bonds to purine bases in a purine·pyrimidine duplex, would provide much greater specificity, and therefore could potentially be used to target specific genes and prevent their transcription (*2*, *3*).

Although the existence of triple-stranded nucleic acids was realized in 1957 (*4*), it was only recently that structural details were revealed for both the parallel and antiparallel helices (*5*−*11*). In all cases, the triplexes for which structural information is available have been intramolecular and involve strands of equal length. This has been necessary as DNA triplexes are intrinsically rather weak; for example, the dissociation constant at 20 °C is in the order of 1 μM for a triplex containing an 11-mer third strand (*12*).

There is abundant evidence that the formation of a triplex is a multistep process that may involve significant and slow conformational rearrangements. Thus, the apparent second-order rate constant for the formation of a short triplex is only about 2×10^3 M^{-1} s^{-1} (*12*−*14*). Further, DNA triplex melting has been reported to occur with a high level of hysteresis (*15*), indicating rather slow kinetic processes. That

†This work was supported by the Medical Research Council and Enzacta Ltd. J.L.A. was supported by a fellowship from the Spanish Ministry of Education. H.S.D. was supported by a studentship from the Cancer Research Campaign.

* To whom correspondence should be addressed: Professor T. C. Jenkins, School of Chemical and Life Sciences, University of Greenwich, Wellington Street, Woolwich, London SE18 6PF, U.K. E-mail: t.c.jenkins@gre.ac.uk. Telephone: [+044] (0)181-331-8209. Fax: [+044] (0)181-331-8305.

‡ National Institute for Medical Research.

§ Institute of Cancer Research.

|| University of Greenwich.

10.1021/bi980057m CCC: $15.00
Published on Web 10/09/1998

Scheme 1: Numbering System Used for the Duplex and Triplex DNA Systems[a]

strand 3 5′-d(**$T^{35}C^{36}T^{37}T^{38}C^{39}T^{40}U^{41}T^{42}C^{43}C^{44}T^{45}$**)—3′

strand 1 5′-d(C^{1} G^{2} C^{3} T^{4} **A^{5} G^{6} A^{7} A^{8} G^{9} $A^{10}A^{11}A^{12}G^{13}G^{14}A^{15}$**$C^{16}G^{17}$)—3′

strand 2 3′-d($G^{34}C^{33}G^{32}A^{31}$**$T^{30}C^{29}T^{28}T^{27}C^{26}T^{25}T^{24}U^{23}C^{22}C^{21}T^{20}$**$G^{19}C^{18}$)—5′

[a] In all cases, the junction and/or triplex orientations refer to that of the purine-rich strand 1 sequence. Boldface denotes the triplex region.

the conformation and/or dynamics of triple helices are different from those of the underlying duplexes is evident from footprinting data. Thus, DNase I cuts duplex DNA exclusively from the minor groove direction, yet a major groove-bound third strand almost completely abolishes the activity of the enzyme (*16*). Furthermore, at the 3′ junction of the triplex and duplex, the rate of cleavage of the phosphodiester bonds by DNase I is greatly enhanced compared with that of the free duplex (*17*). This points to marked changes in the conformation and/or dynamics of the minor groove on forming the triple-stranded structure. To date, little is known about the conformational difference between duplexes and triplexes, and the changes that may occur at their junctions. Molecular modeling studies (*18*) have indicated that there may be a transition from B-like DNA, with S-type sugar puckers in the duplex regions, to a more A-like structure in the triplex regions that would necessitate a kink at the junction site. Further, DNA intercalation by various ligands is favored by the 5′ junction (*2*). However, NMR data show conclusively that the underlying duplexes in triple helices are not characterized by N-type sugars (*5*−*11*, *19*).

We have used a combination of NMR spectroscopy, surface plasmon resonance (SPR[1]), UV melting, and circular dichroism (CD) spectroscopy to characterize the solution properties of an intermolecular DNA triplex consisting of an 11 base third strand and a 17 bp duplex (here termed the 11−17·17 triplex), derived from the previously described aromatase target gene sequence (*14*). To reduce the overlap in the NMR spectrum for the pyrimidine-rich strands, we have replaced one thymine (dT) residue with a uridine (dU) in each of the Watson−Crick (duplex) and Hoogsteen third strands, as shown in Scheme 1, which also shows the numbering scheme that was used. For comparison, selected properties were also evaluated for a truncated 11−15·15 triplex system, where the two consecutive C·G base pairs at the 3′ end of the duplex (i.e., C^{16}·G^{19} and G^{17}·C^{18}) are removed to leave a flush 3′ end for the triplex.

EXPERIMENTAL PROCEDURES

Materials. The three oligodeoxynucleotides were prepared with an Applied Biosystems 391-EP synthesizer using phosphoramidite chemistry, and purified by reversed-phase HPLC using a PRP-1 column (Hamilton Ltd). Each strand was finally >99.5% homogeneous according to capillary gel electrophoresis under denaturing conditions. 5′-Biotinylated oligonucleotides were prepared using biotin CE−phosphoramidite (Perkin-Elmer Applied Biosystems). Following synthesis, the biotinylated oligonucleotide solutions were washed with 1-butanol, and then desalted by size exclusion chromatography using a Sephadex G25 column. No further postsynthesis DNA purification was required as only the full-length sequence is amenable to 5′-biotinylation and, importantly, only the biotin-functionalized oligonucleotides can bind to the streptavidin-coated biosensor surface used for SPR experiments.

Circular Dichroism. CD spectra were recorded on a JASCO spectropolarimeter as described previously (*20*). Titrations were carried out at a fixed concentration of duplex at 15 and 25 °C in aqueous acetate buffer [100 mM sodium acetate (pH 5.1)]. Titration curves were constructed at 217 nm, corresponding to the maximal change in CD signal. Spectral data were analyzed assuming a simple two-state model, using the KaleidaGraph 3.08 program (Synergy Software, Reading, PA) according to the equation

$$\Delta S = \Delta\sigma C_t \tag{1}$$

where ΔS is the observed signal change corrected for the addition of ligand and $\Delta\sigma$ is the difference in intrinsic ellipticity. The concentration of triplex C_t is related to the total concentrations of duplex (d_0) and third strand (t_0) by

$$C_t = 0.5\{(d_0 + t_0 + K_d) - [(d_0 + t_0 + K_d)^2 - 4d_0t_0]^{0.5}\} \tag{2}$$

where K_d is the equilibrium triplex → (duplex + strand) dissociation constant.

UV Melting. Thermal denaturation studies were performed at 260 nm with a Varian-Cary 1G spectrophotometer interfaced to an IBM 750/OS2 computer for data acquisition, and with temperature control using a Peltier heating accessory. Melts were performed in 1 cm path-length quartz cells. Oligonucleotide solutions were prepared in aqueous CNE buffer [10 mM sodium cacodylate, 300 mM NaCl, and 0.1 mM Na_2EDTA (pH 5.2)], using calculated ϵ_{260} absorption coefficients (*21*) of 1.88×10^5 and 1.32×10^5 M(strand)$^{-1}$ cm^{-1} for strand 1 and strand 2 (17-mers), respectively, and 7.37×10^4 M(strand)$^{-1}$ cm^{-1} for the 11-mer strand 3. DNA solutions were dialyzed against CNE buffer for 48 h prior to use. A 200 μM stock solution of the strand 1·strand 2 duplex was prepared by mixing equimolar solutions of each strand, heating to 95 °C, and cooling to room temperature over the course of 18 h. Triplex solutions at the required concentration were prepared by mixing equimolar stock solutions of strand 3 (200 μM) and the preformed duplex, diluting as required, and allowing the mixture to equilibrate at 15 °C for 18 h. Heating runs for the duplex and triplex solutions were performed between 5 and 85 °C, at a scan rate of 1 °C min^{-1} and with optical sampling at 0.1 °C

[1] Abbreviations: bp, base pair; bt, base triplet; CD, circular dichroism; COSY, correlation spectroscopy; ITC, isothermal titration calorimetry; NOESY, nuclear Overhauser enhancement spectroscopy; ROESY, rotating frame Overhauser enhancement spectroscopy; SPR, surface plasmon resonance.

intervals. Analyses of the melting transitions were carried out using the Origin 3.5 program (MicroCal Inc., Northampton, MA) and KaleidaGraph software.

For the 17-mer duplex (10 μM), a transition at 63.5 °C was observed for heat-induced strand separation. In the presence of an equimolar amount of strand 3, a second broader transition appeared at a lower temperature that was dependent on the DNA triplex concentration used [e.g., 35.1 and 63.6 °C at 10 μM(triplex), termed T_m1 and T_m2, respectively]. Thus, the low-temperature T_m1 transition can be attributed to thermal triplex → (duplex + strand) melting and the T_m2 event to strand separation of the host duplex. Thermodynamic van't Hoff parameters (ΔH_{vH}) for triplex formation were obtained by curve fitting (*22*, *23*) the experimental melting data using eqs 2 and 3

$$A_{norm} = \frac{K_d}{2C_t}\left[\left(1 + \frac{4C_t}{K_d}\right)^{0.5} - 1\right] \quad (3)$$

where A_{norm} is the normalized absorbance at 260 nm for the T_m1 transition, and by applying the standard thermodynamic relationships

$$K_d = K_d(T_m1)\exp\left[\frac{-\Delta H_{vH}}{R}\left(\frac{1}{T} - \frac{1}{T_m1}\right)\right] = \exp\left(\frac{\Delta S}{R} - \frac{\Delta H_{vH}}{RT}\right) \quad (4)$$

The concentration-dependent behavior of T_m1 was also used to determine the van't Hoff thermodynamic parameters (*21*) for triplex formation according to eq 5:

$$\frac{1}{T_m1} = \frac{R}{\Delta H_{vH}}\ln(C_t) + \frac{(\Delta S - R\ln 4)}{\Delta H_{vH}} \quad (5)$$

Surface Plasmon Resonance. SPR measurements were taken using a BIAcore 2000 instrument essentially as described previously (*14*). Biosensor chips precoated with streptavidin (SA5 research grade; BIAcore, Stevenage, U.K.) were used for all experiments, and oligonucleotide solutions were prepared in an aqueous TAE running buffer [40 mM Tris-acetate and 5 mM Na_2EDTA (pH 5.2)]. The sensor chip surface was conditioned prior to use by treatment with three serial injections of 1 M NaCl in 50 mM NaOH, and then equilibrated with running buffer at the temperature required for the experiment. A solution of the 5′-biotinylated strand 1 oligomer (100 nM in running buffer) was passed over the sensor chip at 5 μL min^{-1} until the target surface density of the captured oligonucleotide was achieved, corresponding to 200−400 response units (RU). A solution of strand 2 (40 μL at 5 μM) was next passed over the chip surface at 5 μL min^{-1} to effect formation of the duplex with the captured first strand. Solutions containing 1.0, 1.5, 2.0, 3.0, 4.0, 5.0, 12.0, or 20 μM strand 3 were then injected over the immobilized strand 1·strand 2 duplex at a flow rate of 20 μL min^{-1} to generate the 11−17·17 triplex. After each experiment, the surface-bound duplex was regenerated with a 30 s pulse of 10 μM NaOH, followed by an injection of strand 2 (30 μL at 5 μM) and re-equilibration with the TAE running buffer.

The protocol adopted differs in two key respects from that described previously (*14*) for this triplex-generating system. (i) The flow rate used for strand 3 is 4-fold higher so mixing and equilibration could be improved. (ii) Spermine was not used in the running buffer as no effect could be established. (iii) The quantity of strand 1 immobilized on the sensor chip, and hence the captured surface density, is significantly smaller than that (750 RU) used earlier. These modifications were introduced to reduce possible rate-limiting effects upon triplex formation at the chip surface due to mass transport phenomena (*24*, *25*). Experiments were performed at fixed temperatures in the 15−30 °C range. The possible effects of added Mg^{2+} ions upon association behavior at pH 5.2 were separately examined using a modified TAE running buffer containing 5 mM $MgCl_2$, as used in the earlier study (*14*), or equivalent EDTA-free Tris-acetate buffers containing up to 20 mM $MgCl_2$.

Association (capture) curves were fitted to a single-site model using the supplied BIAevaluation 3.0 software as a single exponential (*26*) according to

$$R = R_{max}[1 - \exp(-k_{obs}t)] \quad (6)$$

where R is the instrument response at time t, R_{max} is the maximum response, and k_{obs} is the experimental pseudo-first-order rate constant (*14*, *24*−*26*). This is related to the apparent second-order association [k_a(app)] and first-order dissociation [k_d(app)] rate constants by

$$k_{obs} = k_a(\text{app})[\text{strand 3}] + k_d(\text{app}) \quad (7)$$

where [strand 3] is the concentration of the third-strand oligopyrimidine (see Scheme 1). Direct estimates for k_d were also obtained from first-order fits to sensorgram data acquired during longer times for the slower triplex → duplex and single strand dissociation process (see Figure 2A). Multiple data sets were fitted simultaneously to derive best-fit values for k_a(app) and k_d that described all of the experimental kinetic data.

NMR Spectroscopy. ^{1}H NMR spectra were recorded at 14.1 (≈600 MHz) and 11.75 T (≈500 MHz) using Varian Unity and UnityPlus spectrometers, respectively. Oligonucleotide solutions were prepared in an aqueous phosphate buffer (10 mM NaH_2PO_4 and 100 mM KCl, fixed pH values in the range of 4.8−6.0) for initial experiments, before switching to a superior acetate-buffered system [25 mM sodium acetate-d_3 and 100 mM KCl (pH 5.0)] for all reported spectral acquisitions. In separate studies, the effects of Mg^{2+} were examined using 0−20 mM $MgCl_2$ as a cosolute. The strand 1·strand 2 duplex was made by mixing equal amounts of each strand, according to their optical absorptions at 260 nm (see above), and annealed slowly from 70 °C. Samples for spectroscopy in D_2O were prepared by lyophilizing the solutions, redissolving in D_2O, and adjusting the apparent pH to 5.0 (uncorrected pH meter reading). The triplex was prepared by titration of the duplex with a solution of strand 3 (prepared analogously) and monitoring the NMR spectrum. Working duplex and triplex solutions were each 1 mM in strands. The hypercomplex method (*27*) was used for acquiring phase-sensitive two-dimensional spectra. For experiments in H_2O, the solvent peak was suppressed using the Watergate method (*28*). TOCSY spectra were recorded using MLEV-17 for the spin lock (*29*). ROESY spectra were recorded using a weak continuous wave spin lock field (ca.

4 kHz). Proton-decoupled ^{31}P NMR spectra were recorded at 9.4 T on a Bruker AM400 spectrometer.

^{31}P NMR relaxation rate constants were determined by inversion recovery and spin echo measurements as described previously (*30*, *31*). The rotational correlation times and chemical shift anisotropy were calculated as described previously (*30*). Apparent rotational correlation times were also determined from measurements of the cross-relaxation rate constant for cytosine H6−H5 vectors (*32*, *33*). The exchange rate constant was estimated from the time dependence of the magnetization transfer between triplex and duplex for a resolved cytosine H5 resonance. For an isolated spin undergoing exchange between two states, A and B

$$\mathrm{A} \underset{k_{-1}}{\overset{k_1}{\rightleftarrows}} \mathrm{B} \qquad (8)$$

if the intrinsic spin−lattice relaxation rate constants $\rho(\mathrm{A}) = \rho(\mathrm{B})$, then, from standard formulas (*34*), the ratio r of the cross-peak intensity to that of the summed cross-peak and diagonal peak intensities can be described by

$$r = [\alpha/(1+\alpha)]\{1 - \exp[-k_{-1}(1+\alpha)]t_m\} \qquad (9)$$

where $\alpha = k_1/k_{-1}$ and t_m is the mixing time. NOE volumes were determined using Felix 95.0 (Molecular Simulations Inc., San Diego, CA) by fitting Gaussian peak shapes in cross sections.

Nucleotide conformations were determined as previously described using scalar coupling constants and NOE time courses with the NUCFIT program (*10*, *35*).

RESULTS AND DISCUSSION

Thermodynamics and Kinetics

The equilibrium constant (K_d) for dissociation of the third strand from the DNA triplex was determined using CD, UV melting, and SPR. Figure 1 shows the results for the CD titration of the 17-mer strand 1·strand 2 duplex with the Hoogsteen strand (strand 3) at pH 5.1 and 15 or 25 °C. The maximum change in signal was found to be at 217 nm (Figure 1A). The titration data at 217 nm (Figure 1B) are well described by a simple binding isotherm, and were analyzed according to eqs 1 and 2 (see Experimental Procedures). The dissociation constant K_d values determined from these data were 0.5 ± 0.2 μM at 15 °C and 2.2 ± 0.5 μM at 25 °C, and are comparable to values determined for other 11-mer triplexes from fluorescence studies (*12*). Indeed, the values are comparable to those estimated for similar triplexes using affinity cleavage or filter-binding assay techniques (*13*, *36*). We also estimate a K_d value in the range of 2−10 μM (Table 1) from our NMR data at 40 °C (see below). For comparison, the dissociation constant determined at 25 °C for the truncated 11−15·15 triplex was essentially identical to that for the 11−17·17 triplex system using the same conditions. This indicates that there is no significant thermodynamic effect due to the additional 3′ duplex overhang segment compared to the blunt-ended triplex (but see below).

Thermal denaturation of the 17-mer duplex (10 μM) at pH 5.2 gave a UV melting transition T_m of 63.5 °C. Upon addition of an equimolar amount of the Hoogsteen third strand, a second transition appears, with a T_m of 35.1 °C at 10 μM(triplex) (Figure S1 in the Supporting Information). Each optical event was fully reversible for both heating and cooling at 1 °C min^{-1}, indicating rapid thermal equilibration under these solution conditions. Line shape analysis of the independent melting behaviors, using eqs 3 and 4 and assuming a two-state model for each process, gave a $\Delta H_{vH}1$ of 74.6 ± 1.4 kcal mol(triplex)$^{-1}$ [i.e., 6.8 kcal mol(bt)$^{-1}$] for triplex → (duplex + strand) disruption and a $\Delta H_{vH}2$ of 102.2 ± 0.5 kcal mol^{-1} for the duplex → strands transition. The T_m1 value for 11−17·17 triplex melting was dependent on the concentration in the 0.5−100 μM(triplex) range. From a van't Hoff plot of $1/T_m1$ versus $\ln(C_t)$, the dissociation enthalpy ΔH_{vH} was determined (eq 5) to be 75.6 ± 4.6 kcal

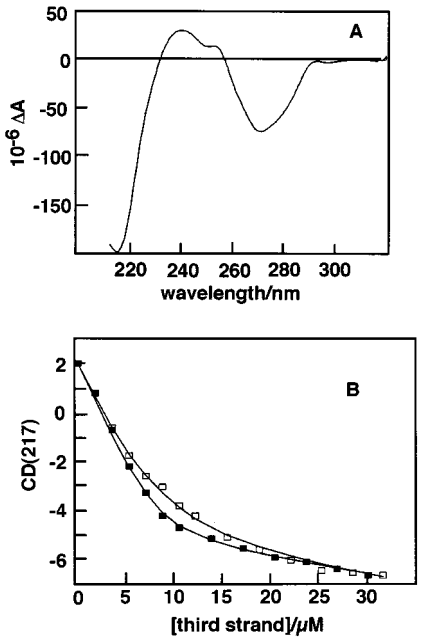

FIGURE 1: CD titration of the strand 1·strand 2 duplex d(CGCT-**AGAAGAAAGGA**CG)·d(GCGA**TCTTCTTTUCCT**CG) with the d(TCTTCTUTCCT) third strand (see Scheme 1). (A) Difference CD spectrum [i.e., triplex − (duplex and third strand)], where ΔA is the difference in absorption of left- and right-circularly polarized light. (B) Titration curves for the induced CD change at 217 nm and 15 (■) or 25 °C (□), with associated fits according to eqs 1 and 2.

Table 1: Thermodynamics and Kinetics of Triplex Formation with the 17-mer Host Duplex[a]

method	T (°C)	K_d (μM)	k_a(app) (M^{-1} s^{-1})	k_d (s^{-1})
SPR[b]	15	0.13	1.37×10^3	1.75×10^{-4}
	25	0.09	2.4×10^3	2.2×10^{-4}
	30	0.12	5.7×10^3	7.1×10^{-4}
CD	15	0.5		
	25	2.2 (1.6)		
UV	25	0.08,[c] 0.51[d]		
	35	5.1		
ITC	25	1.8		
NMR	40	2−10	nd[e]	0.2

[a] Equilibrium constants and rate constants were determined as described (see the text). Values in parentheses refer to the truncated 15-mer duplex. [b] Apparent dissociation constants shown are given by the k_d/k_a(app) ratio at each temperature. [c] Calculated from the K_d value at $T = T_m1$ [i.e., $K_d(T_m1) = C_t/4$] using the van't Hoff relationship (eq 4), with a ΔH_{vH} of 74.6 kcal mol(triplex)$^{-1}$ from UV melting. [d] Dissociation constant calculated similarly, with a $\Delta H°$ of 41.9 kcal mol(triplex)$^{-1}$ from ITC. [e] nd, not determined.

mol(triplex)$^{-1}$, in good agreement with the line shape analyses.

Isothermal titration calorimetry (I. Haq, B. Z. Chowdhry, and T. C. Jenkins, unpublished data) for the association of strand 3 with the strand 1·strand 2 duplex at pH 5.2 in CNE buffer gave an excellent fit to a single-site binding model, with a K_d of 1.8 μM at 25 °C, and with a binding enthalpy $\Delta H°$ of −41.9 kcal mol(triplex)$^{-1}$, or −3.8 kcal mol(bt)$^{-1}$. This enthalpy is similar to values reported for parallel triplexes using calorimetry (*37*, *38*), but lower than values determined by UV melting (*39*, *40*). Disparity between experimental ΔH_{vH} and calorimetric transition enthalpies, particularly from optical melting data, has been reported previously and suggested to reflect an oversimplification in the two-state (i.e., all-or-none) assumption used for van't Hoff analysis (*23*, *37*, *41*, *42*). The calorimetric $\Delta H°$ for the 11−17·17 triplex is also markedly sensitive to temperature in the 10−35 °C range, with a heat capacity change ΔC_p of −0.6 kcal mol^{-1} K^{-1}. This behavior is consistent with reported ΔC_p values of −0.6 and −0.9 kcal mol^{-1} K^{-1} for comparable 15−23·23 DNA triplexes (*36*, *42*), and reinforces possible sources for discrepancy between calorimetric and van't Hoff enthalpies (*43*). Interestingly, such large ΔC_p values contrast with insignificant values for DNA duplexes (*23*, *37*). However, as strand 3 contains four cytosines (Scheme 1) that would each require formal N3 protonation to enable formation of C$^+$-G·C base triplets, the *apparent* calorimetric $\Delta H°$ will be sensitive to both pH and the extent of ionization of the buffering species involved (*44*, *45*). The implicated protons must also be considered as ligands in the triplex association process. At pH 5.2, for example, only approximately 17% of any third-strand cytosine will be protonated (assuming equivalence and a pK_a of 4.5 for an isolated cytosine) and these protons must be supplied by the buffering medium. Hence, the summed protonation enthalpies for the cytosines and the deprotonation enthalpy for the buffer provide additional factors that could also contribute to any divergence between ΔH_{cal} and ΔH_{vH} in such systems.

The UV melting data give a K_d of 5.1 μM at $T = T_m1 =$ 35.1 °C; using the calorimetric $\Delta H°$ enthalpy from ITC, the value of K_d at 25 °C is calculated to be 0.5 μM. Thus, the dissociation constants measured in the CD, UV melting, and calorimetric experiments at 25 °C and pH 5.1−5.2 show good agreement (Table 1). The small variations found can be attributed to a combination of experimental errors, pH differences, and salt effects from the variety of buffer systems used. Of these, slight pH variations are likely to be the most important as parallel triplexes containing multiple C$^+$-C·G triplets are very pH-sensitive (*39*, *40*, *46*), whereas they are only weakly dependent on ionic strength (*37*, *46*). The small variation in K_d is noteworthy given the range of salt concentrations and buffers associated with each technique.

Figure 2 shows a typical series of SPR sensorgrams obtained for the 11−17·17 triplex system. Both the association and dissociation phases of the reaction were well described by a single exponential at every concentration of strand 3 used. The observed rate constant in the triplex-forming phase showed a linear dependence on the concentration of strand 3, where the slope and intercept values give the apparent association and dissociation rate constants, k_a(app) and k_d(app), respectively (eq 7). Because the intercept obtained from linear regression was small, though always positive (Figure 2B), the k_d(app) value could not be accurately determined from the association phase. However, the slow exponential decay phase (shown partially in Figure 2A) independently provides a direct estimate of the dissociation rate constant k_d. Detailed analysis of SPR data for the 11−17·17 triplex system gave rate constants k_a(app) of 2.4 × 10^3 M^{-1} s^{-1} (association) and k_d of 2.2 × 10^{-4} s^{-1} (dissociation) at 25 °C.

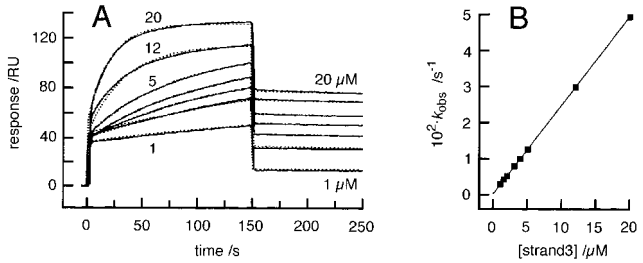

FIGURE 2: SPR sensorgram for triplex-forming hybridization of the 17-mer strand 1·strand 2 duplex d(CGCT**AGAAGAAAGGA**-CG)·d(GCGA**TCTTCTTUCCT**CG) with d(TCTTCTUTCCT) at 25 °C. Experiments were carried out as described in Experimental Procedures for increasing concentrations of strand 3 (1, 1.5, 2, 3, 4, 5, 12, and 20 μM). (A) The rising phase shows the binding (association) process. The continuous lines show raw SPR data for each concentration of injectant, and the dotted curves represent the best single-exponential fits obtained using eq 6. (B) Dependence of the experimental pseudo-first-order rate constant k_{obs} upon the concentration of triplex third strand; the slope gives the apparent second-order association rate constant k_a(app) (cf. eq 7, and see the text).

Measurements at different temperatures in the 15−30 °C range showed that k_d increases strongly with increasing temperature. However, the k_a(app) rate constant determined by this SPR method also increases by approximately the same factor over the temperature range examined (Table 1), indicating "apparent" activation energies of ∼17 kcal mol^{-1} for both processes. This behavior contrasts with a reported decrease of the association rate constant with increasing temperatures for a 15−23·23 DNA triplex, with an activation energy of −8 kcal mol^{-1} and a virtually temperature-independent K_d value in the 5−25 °C range at pH 5.0 (*36*). Although Mg^{2+} ions are known to strongly influence the stability of parallel T-A·T triplexes (*46*, *47*), measurements taken in the presence of added 0−20 mM $MgCl_2$ gave closely similar results for the present triplex (data not shown). Similarly, 10 μM spermine was found to have no significant effect upon the association kinetics, although this concentration of polyamine has been shown by SPR to increase the rate of triplex formation in a T30-A30·T30 system (*14*). These results probably reflect the influence of the dispersed positive charges associated with the N3-protonated cytosines in the Hoogsteen third strand, and contrast with the stabilizing effects of divalent metal ions and polycations upon uncharged, parallel T-A·T triplexes (*46*).

The ratio of the rate constants determined by SPR gives an estimate of the apparent dissociation constant [K_d(app) = k_d/k_a(app) = 0.09 μM at 25 °C] that is essentially independent of temperature in the 15−30 °C range. However, this value is significantly (20-fold) smaller than the K_d value determined by CD and ITC (Table 1), and the temperature independence is not consistent with either the calorimetric or van't Hoff enthalpy (see above). Thus, we

conclude that the equilibrium affinity measured for DNA triplexes by the SPR method is only apparent. As the association rate constant k_a(app) is here similar to values determined by independent fluorescence-based or filter-binding solution methods (*12*, *36*), it is likely that the primary reason for the difference involves the dissociation rate constant, k_d, which is at least 1 order of magnitude smaller than predicted. Mass transport-limiting effects have been suggested to be responsible for the poor estimation of rate constants by SPR compared with values measured in solution (*24*, *25*). This has recently been highlighted in a comparative study of triplex formation using solution and biosensor techniques, where disagreement between the methods was partly ascribed to matrix phenomena, immobilization, and accessibility effects (*48*). We note that k_a(app) is identical to the rate constant previously reported for this triplex system (*14*), whereas our present k_d value is ∼3-fold greater. Experimental factors intended to improve equilibration on the biosensor surface appear to have little influence upon the kinetic parameters. Importantly, k_d/k_a(app) (0.04 μM in ref *14* and 0.09−0.13 μM here) is not directly comparable to the thermodynamic equilibrium dissociation constant. This behavior is as expected for a multistep "zippering" mechanism or non-two-state process in which neither nucleation nor the first elongation steps are completely rate-limiting (*49*), as has previously been suggested for DNA triplexes (*15*).

Comparison of the van't Hoff and calorimetric enthalpy changes (see above) provides further support for a complex binding process. Although agreement between these terms is generally good for DNA duplex ↔ strands denaturation (*22*, *37*, *38*, *50*), there is often a large discrepancy between $\Delta H°$ and ΔH_{vH} for the analogous triplex ↔ (duplex + strand) melting event (*37*−*40*, *42*−*45*). In this study, the apparent calorimetric $\Delta H°$ (3.8 kcal mol(bt)$^{-1}$) is only ∼60% of the ΔH_{vH} value (6.8 kcal mol(bt)$^{-1}$) established from optical melting. We have recently determined ΔH_{vH} values in the 4.3−5.7 kcal mol(bt)$^{-1}$ range for intramolecular triplexes, depending on the base sequence and composition (*40*); ΔH_{vH} values in the 6−8 kcal mol^{-1} range have also been reported (*39*). While some of this variation is due to sequence effects, uncertainty about the protonation status of the triplex must also be an important factor, as this depends on both the position and number of third-strand cytosines together with the solution pH (*40*). Nevertheless, it appears that ΔH_{vH} is generally significantly greater than the calorimetric enthalpy, even for short triplexes.

NMR Spectroscopy

Proton Assignments of the DNA Triplex. Figure 3 shows the spectral region for the exchangeable protons of the 11−17•17 triplex at different temperatures. The protons were assigned using NOESY spectra recorded at 10, 20, and 40 °C using the sequential NOEs between imino protons (12.5−16 ppm) and to C(N4) protons (*51*). As the temperature is raised, certain low-field C(N3H$^+$) resonances (C36 and C43) broaden and disappear by 30 °C, whereas that of C39 remains sharp. The resonances between 9 and 10 ppm showed strong correlations with another resonance in the same region, and also to the C(H5) protons; they can therefore be assigned to the amino protons of cytosines in the third strand. These

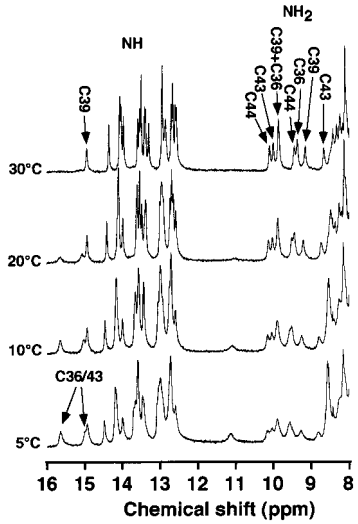

FIGURE 3: NMR spectra for the exchangeable protons. Spectra were recorded at 14.1 T (≈600 MHz) and pH 5.0 (25 mM CD_3CO_2Na and 100 mM KCl) as described. Partial one-dimensional spectra showing the Hoogsteen imino and amino protons of the intermolecular 11−17•17 triplex at different temperatures in the 5−30 °C range.

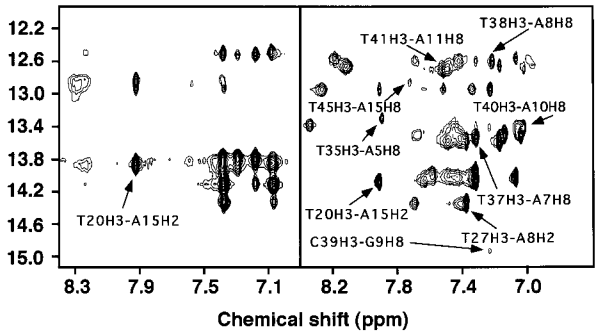

FIGURE 4: NOESY spectra of the 17•17 duplex (left) recorded at 10 °C with a mixing time of 300 ms and the 11−17•17 triplex (right) recorded at 30 °C with a mixing time of 100 ms. Arrows show the cross-strand NOEs within the duplex, and between the third strand and the purine strand.

resonances continue to sharpen as the temperature is raised from 5 to 30 °C. This demonstrates conclusively that a triple helix is present under the conditions of the experiments, and that it is stable at least to 30 °C. In Figure 4, the low-field regions of NOESY spectra are compared for the triplex and duplex; clearly, there are many additional cross-peaks in the triplex spectrum. These were assigned using the NOE interactions, as shown in Figure 4, and by connection to H8 protons in the purine strand. This both verifies the parallel orientation of the third strand with respect to the purine strand and demonstrates that the pairing is via Hoogsteen hydrogen bonds (*51*). Although the spectral quality was good for the 45-nucleotide 11−17•17 triplex in view of the sequence constraints, we expected that the shorter 11−15•15 triplex (41 nucleotides) lacking the 3′ junction would give better spectra, especially as the apparent dissociation constant for the Hoogsteen strand is the same (see above). However, the spectra were considerably poorer, possibly because of aggregation phenomena. The spectral quality was poor even at 40 °C, suggesting that there are unfavorable exchange processes contributing to the line width. We therefore focused on the NMR spectroscopy of the longer 17 bp host duplex molecule.

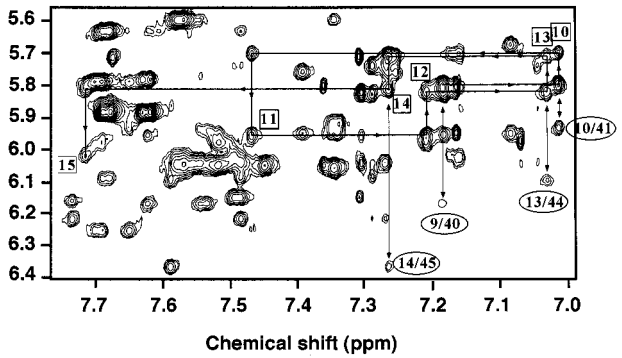

FIGURE 5: NMR assignments in the 11-17·17 triplex. The base−H1′ region of a 300 ms NOESY spectrum in D_2O recorded at 14.1 T (≈600 MHz) and 40 °C is shown. The base proton−H1′ sequential assignments in the purine strand are shown with lines and the nucleotide number in a square box. The cross-strand H8−H1′(n + 1) (i.e., strand 1 to strand 3) NOEs are shown in oval boxes.

In D_2O, the purine resonances were easy to identify by following the standard sequential connectivities involving the base H6/H8−H1′, and H2′/H2″ or H3′ pathways. The H2′ and H2″ were verified by analysis of the correlations between H1′ and H2′/H2″ in both NOESY and DQF-COSY spectra (not shown). The base and sugar protons in the pyrimidine strands were more difficult to assign, but the combination of the NOESY correlations between base and H1′ protons, base-H2′/H2″, and H1′−H2′/H2″ allowed completion of the assignments for the three strands. However, there were additional cross-peaks that could not be assigned to sequential intrastrand interactions (Figure 5). Indeed, they can only be assigned to cross-strand sequential interaction between the purine and Hoogsteen H8−H1′, further demonstrating the presence of a parallel triple helix (*10*, *51*).

We have also assigned the free duplex by standard methods under the same conditions (pH 5.0) used for the triplex. No significant spectral differences were evident for either the duplex or triplex in the presence of 0−20 mM added $MgCl_2$, in agreement with our SPR data showing that Mg^{2+} ions have little influence upon triplex formation. In contrast, NMR spectra for the triplex were sensitive to pH, such that a considerable amount of free duplex was present at pH ≥5.5 and was reduced to ≤10% only at pH 5.0 (see below). Figure 6 shows the changes in proton chemical shifts for the two Watson−Crick strands on forming the 11−17·17 intermolecular triplex. The largest shift perturbations are in purine-rich strand 1, with negative changes for the H8 (major groove) and H2′ (minor groove) protons, and positive changes for H1′ and H2″ (both minor groove). The large changes associated with major groove protons are unsurprising as the third strand interacts directly with the purines of the duplex. The magnitudes of the shift perturbations also increase from outside the triplex (i.e., beyond the triplex−duplex junction), reach a maximum near the center of the triple-stranded region, and then decrease toward the 3′ end of the host duplex sequence.

Chemical shift perturbations in pyrimidine-rich strand 2 were small, but generally larger for minor groove protons than for major groove protons. This observation suggests that there is some perturbation of the minor groove in the triplex region. Also, the H1′ shifts are consistently larger

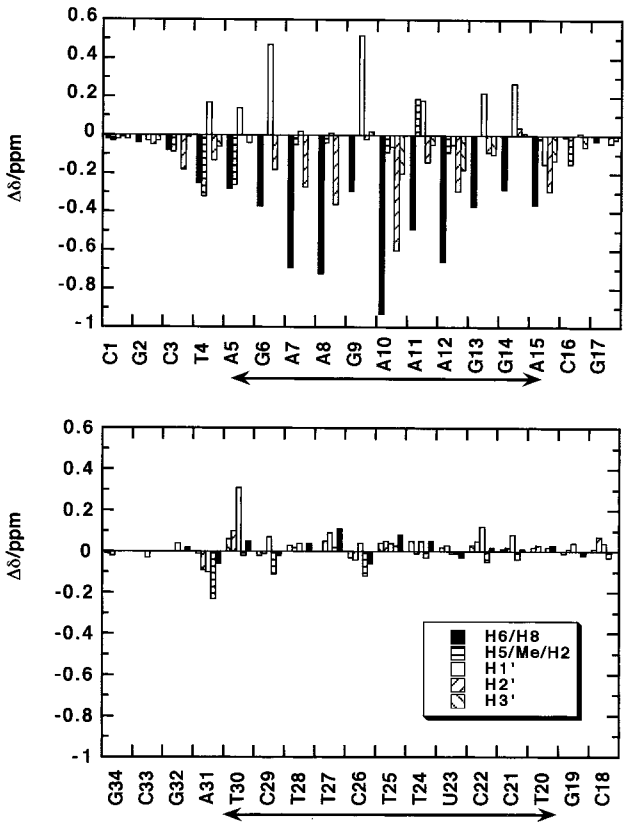

FIGURE 6: Proton chemical shift differences at 40 °C for the host 17-mer (strand 1·strand 2) duplex d(CGCT**AGAAGAAAGGA**CG)·d(GCGA**TCTTCTTTUCCT**CG) with or without d(TCTTCTUTCCT). The double-headed arrows denote the position of the third strand.

in the C^+-G·C triplets than in the T-A·T base triplets. Very similar patterns of shifts were observed for an intramolecular triplex and the corresponding duplex host (*10*). However, at the 5′ end of the junction (reading along purine-rich strand 1), not only do the shift perturbations extend beyond the start of the triplex region, but there are also distinct perturbations at the junction site that are particularly evident in Watson−Crick pyrimidine strand 2 (Figure 6). Thus, the two residues at the junction site show opposite patterns of chemical shift perturbations. No similar perturbation is found at the 3′ end, though this may be because the duplex only extends a further 2 bp. However, this is also consistent with our CD data indicating that the 2-bp duplex extension at the 3′ end does not significantly influence the overall thermodynamic stability. Nevertheless, the shift data indicate an alteration in the duplex conformation upon binding the third strand and that there is some induced perturbation, at least at the 5′ junction.

Triplex Dynamics. The equilibrium data indicate that at strand concentrations of 1 mM, up to 10% of the triplex will be dissociated at 40 °C. A ROESY spectrum recorded in D_2O at 40 °C (not shown) reveals exchange peaks between the assigned triplex and duplex resonances, which conclusively demonstrates that there is an equilibrium between the triplex and dissociated (duplex and strand) states and that they are in slow exchange on the chemical shift time scale. Although the spectral overlap is quite severe, we have estimated the relative concentrations of the triplex and duplex from NOESY spectra, from which we obtain an estimate for K_d of 2−10 μM. This is in accord with our CD, UV melting, and ITC data (see above).

Table 2: Values of $\Sigma_{1'}$ in the 17-mer Duplex d(CGCT**AGAAGAAAGGA**CG)·d(CG**TCCUTTCTTCTAGCG**)[a]

nucleotide	$\Sigma_{1'}$	f_S	nucleotide	$\Sigma_{1'}$	f_S
C1	13.7	0.68	C16	14.3	0.78
T4	14.9	0.87	C18	13.7	0.68
A5	**14.9**	**0.87**	G19	14.3	0.78
G6	**15.0**	**0.89**	**T20**	**14.3**	**0.78**
G9	**14.3**	**0.78**	**C22**	**13.7**	**0.68**
G14	**14.9**	**0.87**	**U23**	**14.3**	**0.78**
A15	**14.3**	**0.78**			

[a] The S fraction was calculated (*53*) using $f_S = (\Sigma_{1'} - 9.8)/5.9$. Boldface values refer to the triplex-forming segment.

The presence of the exchange cross-peaks in the ROESY spectrum ($t_{mix} = 50$ ms) indicates an exchange rate constant in the order of $1-10$ s^{-1} at 40 °C. Cytosine 16, whose diagonal peak is resolved in one-dimensional spectra, shows an exchange cross-peak for its H5 resonance. For an isolated spin, and assuming that the spin−lattice relaxation rate constant for the C(H5) proton is similar in the duplex and triplex states, as would be expected on the basis of the similar correlation times, the ratio of the cross-peak intensity to that of the summed diagonal and cross-peak intensities has a simple dependence on the exchange rate constants and mixing time. Fitting the data to eq 9 gave a value of 2 ± 1 s^{-1} for $k_{-1}(1 + \alpha)$ at 40 °C. This is reasonable, given that the fraction of magnetization exchange is ∼1% at a mixing time of 100 ms, and the relative concentrations of triplex and duplex states are in the 10−20 :1 range. From the initial slope, we estimate that $k_d \approx 0.2$ s^{-1}. Even if a substantial underestimation of the dissociation rate constant by SPR is allowed for (see above), this indicates a high activation energy for the triplex dissociation, which would be expected as the activation energy must be larger than the equilibrium enthalpy. This strong temperature dependence of k_d should be kept in mind in any discussion of slow dissociation for DNA triplexes (*15*).

The apparent rotational correlation times were measured using ^{1}H−^{1}H cross-relaxation for the 17-mer triplex (*32*, *33*) and ^{31}P relaxation (*30*, *31*) for both the duplex and the triplex. Correlation times of 6.4 ± 0.5 (triplex) and 5.6 ± 0.3 ns (duplex) were determined from the ^{31}P NMR relaxation data, and 4.3 ± 0.6 ns for the triplex from proton cross-relaxation. These correlation times are similar to those expected for oligonucleotides of this size (*33*). It is commonly found that the rotational correlation time determined from ^{31}P NMR relaxation is larger than that from proton cross-relaxation (*30*, *33*, *52*).

Structural Conclusions. The NMR spectrum of the 11−17•17 DNA triplex is crowded, especially for the pyrimidine strands. However, the resolution of the purine strand in both the duplex and triplex states is surprisingly good. We have been able to determine values of $\Sigma_{1'}$ for some of these residues in the duplex using COSY spectroscopy (Table 2), and also cross-peak volumes from NOESY spectra. According to the $\Sigma_{1'}$ values, the purine nucleotides are primarily in the S domain in the duplex. The pyrimidine nucleotides have lower values of $\Sigma_{1'}$, which is consistent with a greater degree of flexibility as is commonly observed in DNA duplexes (*53*). The resolution in the triplex is poorer, and the resonances are somewhat broader due to the slightly higher correlation time. However, cross-peaks between H1′

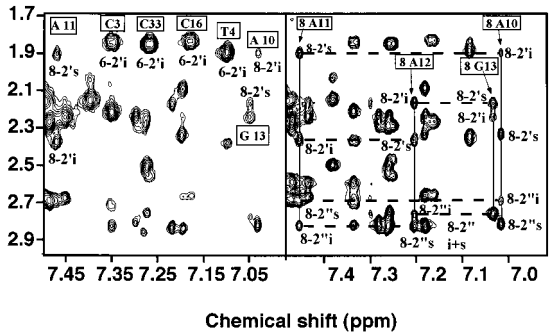

FIGURE 7: NMR spectra of the 11−17•17 triplex in D_2O. Base−H2″/H2′ region of a 50 ms ROESY (left) and a 300 ms NOESY (right) spectrum in D_2O. The nucleotide is shown in a square box (base−proton shift, F2 axis). Cross-peaks are labeled as 8−2′i or 8−2′s, etc., denoting an intranucleotide NOE between the base proton and the H2′/H2″ or a sequential NOE between the base proton of residue *n* and the H2′/H2″ of residue ($n - 1$), respectively.

and both the H2′ and H2″ protons are present in the DQF-COSY spectrum, which is not possible for an N-type sugar. For the purines, the H1′−H2′ COSY cross-peaks are more intense than the H1′−H2″ cross-peaks, indicating that $^3J_{1'2'} > {}^3J_{1'2''}$ and they are predominantly S sugars. In contrast, in the third strand, the two cross-peaks are nearly equally intense for many of the residues, such that $^3J_{1'2'} \approx {}^3J_{1'2''}$. This indicates that the Hoogsteen pyrimidine sugars have a significant contribution from N-type puckers, which is supported by the noticeably stronger NOEs evident for H3′−H6 compared to H3′−H8 in the purines. In addition, the intranucleotide NOEs are consistent with predominantly S-type sugar conformations (purines) and anti glycosyl torsion angles (and see below). Therefore, the sugars in the triplex state must largely have conformations that are on average similar to those in the free duplex, as we have previously observed in a comparison of an intramolecular triplex with the corresponding duplex (*10*).

Particularly relevant to structural features are the intranucleotide H2′/H3′−H8 and internucleotide H2′/H2″-H8 NOEs. In general, the intranucleotide H2′−H8 NOE is more intense for the duplex than the triplex. In addition, the sequential H2″−H8 NOE is more intense than the H2′−H8 NOE in the duplex, but these NOEs are more similar for some steps in the triplex. This is particularly clear for A10 (Figure 7), where the intranucleotide H8−H2′ NOE intensity is low, indicating a glycosyl torsion angle that is different from the average value found in DNA duplexes (i.e., −140° to −160° vs −100° to −120°). The sequential NOE A2-(H2′)−A11(H8) is comparable to that of the A11 intranucleotide NOE, which is not the pattern observed in duplex DNA in solution, indicating a different helical arrangement at this step (and others, cf. Figure 5). Together with the other NOE data, and the limited coupling results, this is consistent with a typical range of S sugars and glycosyl torsion angles in the duplex state, and somewhat smaller phase angles, a lower fraction (f_S) of the S conformation, and a larger glycosyl torsion angle in the triplex state. Where the resolution was sufficient, we have measured the time dependence of the intranucleotide NOEs, and used NUCFIT (*35*) to determine the glycosyl torsion angles (χ), as shown in Table 3. Because of the strong dependence of χ on the H6/H8−H2′ NOE, the glycosyl torsion angles found for each nucleotide are determined within an interval of ca. 10−20°. As Table 3

Table 3: Glycosyl Torsion Angles in the 11−17·17 DNA Triplex[a]

nucleotide	$-\chi$ (deg)	nucleotide	$-\chi$ (deg)	nucleotide	$-\chi$ (deg)
G2	100−110	A12	120−130	T20	90−110
C3	110−120	G13	110−130	T30	100−110
A5	110−120	C16	110−120	A31	100−110
A10	140−150	G17	105−125	T35	110−120
A11	100−120	G19	115−125	C36	120−130

[a] Torsion angles (χ) were determined from NOE time courses with the program NUCFIT (*35*), as described. Values are given as the angle range accounting for the data.

shows, the χ angles of some of the nucleotides in the triplex state are larger than those in the duplex portions, or in duplex DNA generally. These small but significant differences are also consistent with the observed triplex-forming induced changes in proton chemical shifts (see above). We have recently shown that there are small but significant changes in χ-angles between the triplex and duplex states for a short intramolecular triplex, and that these changes correlate with the large changes in chemical shifts (*10*).

Only the resonances in the purine strand are sufficiently resolved to provide a reasonable number of constraints. Models based on the available NOEs show that the purine strand is relatively well determined, and that overall the triplex is similar to structures reported for intramolecular parallel triple helices (*7*−*11*). A complete NOE-based structure calculation of the entire triplex is not warranted by the data, however.

Table 4 shows the assigned interstrand NOEs in the 17-mer DNA triplex, chiefly between protons in strand 3 and the purine-rich strand 1. These include NOEs that are characteristic for parallel Y−R·Y triplexes, i.e., NOEs between the Hoogsteen imino protons and H8 of the purine in the same triplet, as well as to H2′ and H2″ of the 5′ adjacent nucleotide, and also between the purine H8 and the H1′ protons of the 3′ neighboring Hoogsteen nucleotide (*51*).

In a recent X-ray structure of a partial DNA triplex (*54*), the Hoogsteen bases lie substantially out of the plane formed by the Watson−Crick base pairs. In the published solution NMR structures for parallel triplexes that do not contain mismatches or modified bases (*10*, *11*), the Hoogsteen bases also lie out of the plane, though no NOEs were reported that directly determine this noncoplanarity. In this case, we observe NOEs between T(Me) and C(H5) on Hoogsteen strand 3 bases with T(Me)/C(H5) on (Watson−Crick) pyrimidine strand 2, but two base triplets removed in the 3′ direction (Table 4 shows three such NOEs). These were observed even at a mixing time of 50 ms. For a canonical structure, where the three bases of a triplet are coplanar, the distance between these protons would be approximately 7 Å, which is beyond the limit of detectability for NOEs in these molecules. Further, there is no obvious spin-diffusion pathway that would produce any significant magnetization transfer between these protons. Full relaxation matrix calculations on model structures with coplanar bases were carried out to verify that these NOEs are not observable at these mixing times. In contrast, in structures where there is a significant buckle of the Hoogsteen base that shortens this distance to <5 Å, significant NOEs of this kind could be present. Hence, the observed NOEs imply that the actual distance in the present triplex is less than ∼5 Å, which is consistent with the Hoogsteen bases buckling out of the plane and approaching the base triplet below in the sequence. This buckling also makes possible long, weak hydrogen bonds, analogous to those proposed between neighboring base pairs in oligo(dA)·oligo(dT) structures (*55*), between C(N4) or T(O2) of the Hoogsteen base and one residue below in the sequence context AG or GA, but not in either AA or GG.

Table 4: Interstrand NOEs in the DNA Triplex[a]

strand 1	strand 2	strand 3
T4(H2′,H2″)		T35(N3H)
T4(Me)		T35(H6)
T4(Me)		T35(Me)
A5(H8)		T35(N3H)
	T28(Me)	T35(Me)
	C29(N4H1)	C36(N4H1)
A5(H8)		C36(H1′)
G6(H8)		T37(H1′)
G6(H2′,H2″)		T37(N3H)
A7(H8)		T37(N3H)
A7(N6H1,H2)		T37(N3H)
A7(H8)		T38(N3H)
A7(H8)		T38(H1′)
A7(H2′,H2″)		T38(N3H)
A8(H8)		T38(N3H)
A8(N6H1,2)		T38(N3H)
A8(H8)		C39(H1′)
G9(H8)		C39(N3H$^+$)
	C26(N4H1)	C39(N4H1)
G9(H8)		T40(N3H)
A10(H8)		T40(N3H)
G9(H2′,H2″)		T40(N3H)
G9(H8)		T40(H1′)
A10(H8)		U41(H1′)
A10(H2′,H2″)		U41(N3H)
A10(H8)		U41(N3H)
A11(H8)		U41(N3H)
A11(N6H1,2)		U41(N3H)
A11(H2′)		T42(N3H)
A11(H8)		T42(N3H)
A12(H8)		T42(N3H)
A12(N6H1,2)		T42(N3H)
	C21(H5)	T42(Me)
	T20(Me)	C43(H5)
	C21(N4H1,2)	C43(N4H1,2)
	C22(N4H1,2)	C43(N4H1,2)
	C21(N4H1)	C44(N4H1,2)
A12(H8)		C43(H1′)
G13(H8)		C44(H1′)
G14(H8)		T45(H1′)
A15(H8)		T45(N3H)

[a] The base numbering system is shown in Scheme 1.

The differences in the NOE peak volumes between the triplex and duplex are smaller outside the junction regions, indicating that the molecule soon reverts to its normal DNA duplex conformation. However, the 5′ and 3′ junctions are not equivalent as, at the 5′ junction, the strong NOEs and ROEs between T4 and T35 indicate stacking of the terminal Hoogsteen residue on the first base in the duplex portion before the junction (see Table 4).

CONCLUSIONS

Equilibrium thermodynamic measurements taken for this DNA triplex system using CD, UV melting, and calorimetric methods are mutually consistent and indicate that $K_d = 2 \pm 0.5$ μM at 25 °C and pH 5.1−5.2, with a ΔH_{vH} of 75 kcal mol^{-1} and an *apparent* $\Delta H°$ of 42 kcal mol^{-1}. The enthalpic

discrepancy may in part be related to a markedly temperature-dependent $\Delta H°$ term ($\Delta C_p = -0.6$ kcal mol^{-1} K^{-1}), as established for other intermolecular triplexes (*36*, *42*), and hence that the two-state (all-or-none) assumption used in van't Hoff analyses may not be appropriate for triplex formation. Previous studies indicate that such large ΔC_p values cannot be readily explained in terms of binding-related changes in solvent-accessible surface area for the reactants (*42*), indicating that temperature-related changes in microstate populations may also be important. This conclusion contrasts with that for duplex formation from short single strands, where $\Delta H_{cal} \approx \Delta H_{vH}$, and $\Delta C_p \approx 0$ (*22*, *37*, *38*, *41*, *50*). In this respect, however, thermodynamic factors involving ionization of the buffer and protonation of the third-strand cytosines required to form C^+-G·C triplets must also contribute to any apparent divergence (*44*, *45*), particularly the enthalpy terms associated with cytosine N3-protonation and buffer deprotonation. Triplex formation is clearly rather more complex than implied by a "simple" binding model involving a host DNA duplex and a third complementary DNA strand.

These and previous SPR measurements evidently greatly underestimate the dissociation rate constant k_d compared to the value in free solution, by at least 20-fold. Poor kinetic correspondence here probably arises from factors involving rate-limiting mass transport phenomena (*24*, *25*), and effects that largely stem from immobilization of the triplex-forming duplex on the biosensor surface (*48*). Comparison with kinetic data accumulated for other triplex systems using alternative biophysical techniques suggests that dissociation must be a rather complicated process.

The conformation adopted by the intermolecular 11−17·17 DNA triplex is consistent with published structures for intramolecular triplexes derived from a larger quantity of NMR data, although there is experimental evidence for noncoplanarity of the base triplets in the present system. Clearly, the underlying conformation of the host duplex is not greatly perturbed by binding with the oligopyrimidine third strand, although significant induced changes were noted for nucleotides in the purine strand (compared to the duplex). Any induced changes in conformation are not propagated far beyond the overhang junctions between the triplex and the duplex, in contrast to conclusions based on molecular modeling and electrophoretic behavior (*18*). The 3′ end triplex−duplex junction shows localized perturbations in proton chemical shifts, whereas the 5′ junction shows only a gradual change, suggesting structural differences for the junctions. This is also shown by the NOEs between the first 5′ Hoogsteen base and the first pyrimidine in the duplex portion, indicating stacking interactions. This structural asymmetry for the two junctions may be related to the observed differences in intercalation of drugs to oligonucleotides (*56*) and to DNase I hypersensitivity (*16*).

ACKNOWLEDGMENT

We thank Dr. Ihtshamul Haq (University of Greenwich) for providing ITC data prior to publication. We are grateful to Sanj Kumar and Sylvie Cot (BIAcore, Stevenage, U.K.) for helpful discussions and generous access to the high-performance SPR instrument.

SUPPORTING INFORMATION AVAILABLE

Three figures showing a UV melting curve for the triplex, a DQF-COSY spectrum (17·17 duplex), and a NOESY exchange spectrum (11−17·17 triplex) and two tables of ^{1}H NMR assignments (9 pages). Ordering information is given on any current masthead page.

REFERENCES

1. Searle, M. S. (1993) *Prog. NMR Spectrosc. 25*, 403−480.
2. Sun, J.-S., and Hélène, C. (1993) *Curr. Opin. Struct. Biol. 3*, 345−356.
3. Frank-Kamenetskii, M. D., and Mirkin, S. M. (1995) *Annu. Rev. Biochem. 64*, 65−95.
4. Felsenfeld, G., Davies, D. R., and Rich, A. (1957) *J. Am. Chem. Soc. 79*, 2023−2024.
5. Radhakrishnan, I., and Patel, D. J. (1993) *Structure 1*, 135−152.
6. Radhakrishnan, I., and Patel, D. J. (1994) *Structure 2*, 17−32.
7. Radhakrishnan, I., and Patel, D. J. (1994) *Biochemistry 33*, 11405−11415.
8. Ji, J., Hogan, M. E., and Gao, X. (1996) *Structure 4*, 425−435.
9. Koshlap, K. M., Schultze, P., Brunar, H., Dervan, P. B., and Feigon, J. (1997) *Biochemistry 36*, 2659−2668.
10. Bartley, J. P., Brown, T., and Lane, A. N. (1997) *Biochemistry 36*, 14502−14511.
11. Tarköy, M., Phipps, A. K., Schultze, P., and Feigon, J. (1998) *Biochemistry 37*, 5810−5819.
12. Yang, M., Ghosh, S. S., and Millar, D. P. (1994) *Biochemistry 33*, 15329−15337.
13. Singleton, S. F., and Dervan, P. B. (1992) *Biochemistry 31*, 10995−11003.
14. Bates, P. J., Dosanjh, H. S., Kumar, S., Jenkins, T. C., Laughton, C. A., and Neidle, S. (1995) *Nucleic Acids Res. 23*, 3627−3632.
15. Rougée, M., Faucon, B., Mergny, J. L., Barcelo, F., Giovanangeli, C., Garestier, T., and Hélène, C. (1992) *Biochemistry 31*, 9269−9278.
16. Cassidy, S. A., Strekowski, L., Wilson, W. D., and Fox, K. R. (1994) *Biochemistry 33*, 15338−15347.
17. Chandler, S. P., Strekowski, L., Wilson, W. D., and Fox, K. R. (1995) *Biochemistry 34*, 7234−7242.
18. Chomilier, J., Sun, J.-S., Collier, D. A., Garestier, T., Hélène, C., and Lavery, R. (1992) *Biophys. Chem. 45*, 143−152.
19. Macaya, R. F., Schultze, P., and Feigon, J. (1992) *J. Am. Chem. Soc. 114*, 781−783.
20. Lane, A. N., Martin, S. R., Ebel, S., and Brown, T. (1992) *Biochemistry 31*, 12083−12086.
21. Cantor, C. R., Warshaw, M. W., and Shapiro, H. (1970) *Biopolymers 9*, 1059−1077.
22. Xodo, L. E., Manzini, G., and Quadrifoglio, F. (1990) *Nucleic Acids Res. 18*, 3557−3564.
23. Breslauer, K. J. (1994) in *Methods in Molecular Biology, Volume 26: Protocols for Oligonucleotide Conjugates* (Agrawal, S., Ed.) pp 347−372, Humana Press, Totowa, NJ.
24. Schuck, P. (1997) *Annu. Rev. Biophys. Biomol. Struct. 26*, 541−566.
25. Schuck, P., and Minton, A. P. (1996) *Anal. Biochem. 240*, 262−272.
26. Karlsson, R., and Fält, A. (1996) *J. Immunol. Methods 200*, 121−133.
27. States, D. J., Haberkorn, R. A., and Ruben, D. J. (1982) *J. Magn. Reson. 48*, 286−292.
28. Piotto, M., Saudek, V., and Sklenar, V. (1992) *J. Biomol. Struct. 2*, 661−665.
29. Bax, A., and Davis, D. G. (1985) *J. Magn. Reson. 65*, 355−360.
30. Forster, M. J., and Lane, A. N. (1990) *Eur. Biophys. J. 18*, 347−355.
31. Gyi, J. I., Conn, G. L., Lane, A. N., and Brown, T. (1996) *Biochemistry 35*, 12538−12548.

32. Lane, A. N., Lefèvre, J.-F., and Jardetzky, O. (1986) *J. Magn. Reson. 66*, 201−218.
33. Birchall, A. J., and Lane, A. N. (1990) *Eur. Biophys. J. 19*, 73−78.
34. Ernst, R. R., Wokaun, A., and Bodenhausen, G. (1987) *Principles of Nuclear Magnetic Resonance in One and Two Dimensions*, Chapter 4, Oxford Science Publications, Oxford, U.K.
35. Lane, A. N. (1990) *Biochim. Biophys. Acta 1049*, 189−204.
36. Shindo, H., Torigoe, H., and Sarai, A. (1993) *Biochemistry 32*, 8963−8969.
37. Plum, G. E., and Breslauer, K. J. (1995) *J. Mol. Biol. 248*, 679−695.
38. Scaria, P. V., and Shafer, R. H. (1996) *Biochemistry 35*, 10985−10994.
39. Roberts, R. W., and Crothers, D. M. (1996) *Proc. Natl. Acad. Sci. U.S.A. 93*, 4320−4325.
40. Asensio, J. L., Dhesai, J., Bergqvist, S., Brown, T., and Lane, A. N. (1998) *J. Mol. Biol. 275*, 811−822.
41. Breslauer, K. J. (1985) *Thermodynamic Data for Biochemistry and Biotechnology*, pp 377−394, Academic Press, New York.
42. Kamiya, M., Torigoe, H., Shindo, H., and Sarai, A. (1996) *J. Am. Chem. Soc. 118*, 4532−4538.
43. Naghibi, H., Tamura, A., and Sturtevant, J. (1995) *Proc. Natl. Acad. Sci. U.S.A. 92*, 5597−5599.
44. Wilson, W. D., Hopkins, H. P., Mizan, S., Hamilton, D. D., and Zon, G. (1994) *J. Am. Chem. Soc. 116*, 3607−3608.
45. Husler, P. L., and Klump, H. H. (1995) *Arch. Biochem. Biophys. 317*, 46−56.
46. Soyfer, V. N., and Potaman, V. N. (1996) *Triple-Helical Nucleic Acids*, Springer-Verlag, New York.
47. Pilch, D. S., Levenson, C., and Shafer, R. H. (1990) *Proc. Natl. Acad. Sci. U.S.A. 87*, 1942−1946.
48. Sun, J.-S., Giovannangeli, C., Garestier, T., and Hélène, C. (1995) *Fifth European BIAsymposium*, Stockholm, Sweden, September 27−29, 1995.
49. Cantor, C. R., and Schimmel, P. R. (1980) *Biophysical Chemistry, Part III: The Behavior of Biological Macromolecules*, pp 1239−1289, W. H. Freeman, San Francisco, CA.
50. Xodo, L. E., Manzini, G., Quadrifoglio, F., van der Marel, G. A., and van Boom, J. H. (1991) *Nucleic Acids Res. 19*, 5625−5631.
51. Feigon, J., Koshlap, K. M., and Smith, F. W. (1995) *Methods Enzymol. 261*, 225−255.
52. Lane, A. N. (1995) *Methods Enzymol. 261*, 413−435.
53. van Wijk, J., Huckriede, B. D., Ippel, J. H., and Altona, C. (1992) *Methods Enzymol. 211*, 286−306.
54. Nunn, C. M., Trent, J. O., and Neidle, S. (1997) *FEBS Lett. 416*, 86−89.
55. Nelson, H. C. M., Finch, J. T., Luisi, B. F., and Klug, A. (1987) *Nature 330*, 221−226.
56. Collier, D. A., Mergny, J.-L., Thuong, N. T., and Hélène, C. (1991) *Nucleic Acids Res. 19*, 4219−4224.

BI980057M